Inorganic Chemistry
Article
Cite This: Inorg. Chem. XXXX, XXX, XXX−XXX
pubs.acs.org/IC

Ruthenium(II)-Polypyridyl Compounds with π-Extended Nitrogen Donor Ligands Induce Apoptosis in Human Lung Adenocarcinoma (A549) Cells by Triggering Caspase-3/7 Pathway

Bruno Peña,[†] Sayan Saha,[†] Rola Barhoumi,[‡] Robert C. Burghardt,[‡] and Kim R. Dunbar*[,†]

[†]Department of Chemistry, Texas A&M University, College Station, Texas 77843, United States
[‡]Department of Veterinary Integrative Biosciences, Texas A&M University, College Station, Texas 77843, United States

Supporting Information

ABSTRACT: Ru(II)-polypyridyl complexes exhibit antitumor properties that can be systematically tailored by means of adjusting the ligand environment. In this work, the effect of incorporating π-extended moieties into anionic N^O$^-$ based chelating ligands on the cytotoxic properties of Ru compounds is explored. Four new Ru(II) complexes, $[Ru(bpy)_2(dphol)][PF_6]$ (**1**; bpy = 2,2′-bipyridine, dphol = dibenzo[*a*,*c*]phenazin-10-olate), $[Ru(phen)_2(dphol)][PF_6]$ (**2**; phen = 1,10-phenanthroline), $[Ru(bpy)_2(hbtz)][PF_6]$ (**3**; hbtz = 2-(benzo[*d*]thiazol-2-yl)phenolate), and $[Ru(phen)_2(hbtz)][PF_6]$ (**4**) were synthesized and thoroughly characterized. *In vitro* cytotoxicity was investigated in human lung adenocarcinoma (A549) cells, which revealed that **4** is the most cytotoxic compound (IC_{50} = 0.8 μM) in the series including a control compound $[Ru(bpy)_2(quo)][PF_6]$ (**5**; quo = 8-hydroxyquinolinate) and is nearly 8-fold more cytotoxic than cisplatin. An investigation of the mechanism of cell death led to the finding that compounds **1**−**4** disrupt the mitochondrial transmembrane potential ($\Delta\Psi_m$) in a concentration-dependent fashion, which is an event associated with the intrinsic pathway of apoptosis. Moreover, compound **4** triggers the activity of caspase-3/7, which eventually induces the apoptotic cellular death of A549 cells. Thus, increasing the overall lipophilicity of the Ru compounds by introducing π-extended moieties in the anionic N^O$^-$ ligand is a successful strategy for realizing a new family of pro-apoptotic compounds with a $[Ru^{II}N_5O]^+$ coordination environment.

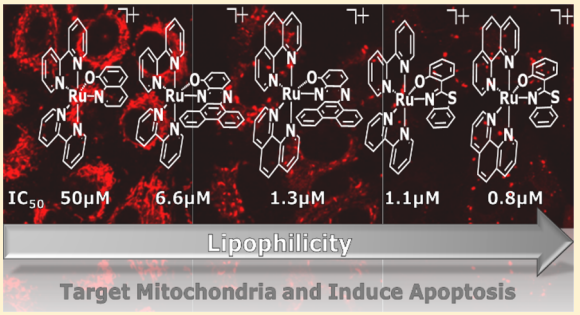

INTRODUCTION

Cancer is a disease characterized by uncontrolled cellular growth and has been one of the leading causes of death globally for the past few decades. In fact it is the second leading cause of death in the United States after heart related disease. Since the fortuitous discovery of cisplatin, *cis*-$Pt(NH_3)_2Cl_2$ in the late 1960s, inorganic cancer chemotherapy is still largely dependent on the administration of Pt-based chemotherapeutic drugs. Despite its success and high cure rates, specifically against metastatic testicular and ovarian cancer, cisplatin suffers from detrimental dose-limiting side effects and tumor resistance.[1,2] To circumvent the undesired limitations associated with Pt drugs, researchers are actively searching for alternative therapies involving different transition metals to produce drugs with lower systemic toxicity and higher selectivity.

Over the past two decades, ruthenium compounds have emerged as promising anticancer agents due to their lower toxicities and effectiveness against Pt resistant tumors. The initial success of NAMI-A and KP1019, both currently in advanced phases of clinical trials, sparked intense investigation of Ru compounds in cancer chemotherapy.[3−8] Ruthenium compounds are a suitable choice for medicinal applications owing to several factors: (a) they form thermodynamically stable coordination compounds with slow ligand exchange rates enabling them to reach biological targets without being modified; (b) they exhibit multiple oxidation states that are stable under physiological conditions; and (c) they are capable of mimicking iron binding for transportation, resulting in lower toxicities.[9,10]

Within the realm of anticancer compounds, Ru(II) polypyridyl complexes are well established for their antitumor properties and are known to inhibit tumor growth by triggering apoptotic/necrotic pathways of cellular death when interacting with mitochondria, the nucleus, and other cell organelles.[11−15] They interact with key cellular targets, including DNA and proteins,[16−19] and can be engineered to release biologically active molecules inside the cell using light. It is also possible to tune their cytotoxicity and cellular uptake simply by modifying the coordination environment through proper choice of ancillary ligands, thereby providing a rich platform for the development of a variety of new drugs. Although the choice of ligand environment provides an ample field to explore, it is

Received: July 15, 2018

DOI: 10.1021/acs.inorgchem.8b01988
Inorg. Chem. XXXX, XXX, XXX−XXX

surprising that most of the reports on the biological activity of octahedral Ru(II) polypyridyl molecules have focused mainly on substitutionally inert complexes that possess neutral N-donor ligands ($[Ru^{II}N_6]^{2+}$),[20−22] with much less focus on other donor atoms.

One advantage of using anionic donor ligands is that the lipophilicity and thus the cellular uptake of the compound increases due to a decrease of the overall charge on the complex. Only a few studies on the cytotoxicity of Ru complexes possessing anionic N^O$^-$ bidentate ligands and a $[Ru^{II}N_5O]^+$ coordination environment are reported in the literature. Meggers et al. used a combinatorial, high throughput screening approach that led to the discovery of [Ru(*t*-Bu_2bpy)$_2$(phox)][PF_6] (*t*-Bu_2bpy = 4,4′-di-*tert*-butyl-2,2′-bipyridine; phox = deprotonated 2-(2′-hydroxyphenyl)-oxazoline) which exhibits low micromolar IC_{50} values in HeLa cervical cancer cells and was found to decrease the mitochondrial membrane potential of Burkitt-like lymphoma (BJAB) cells, suggesting the involvement of the intrinsic pathway of apoptosis.[23] Glazer et al. reported that coordination of hydroxyquinolines to Ru-centers leads to a marked increase in their cytotoxicity through rapid processes which induces apoptosis,[24] whereas Liu and coworkers have shown 8-hydroxyquinoline Ru(II)-complexes can inhibit angiogenesis and *in vivo* tumor growth of HepG2 (human hepatocellular liver carcinoma cells) xenografted on mouse through ERK and AKT signaling pathways.[25] On a different note, Wang et al. explored the non-innocent behavior of Ru-hydroxyquinoline complexes which exhibited DNA photocleavage upon visible light irradiation through a radical mediated pathway that can be utilized in photodynamic therapy (PDT).[26,27]

To expand the library of $[RuN_5O]^+$ cytotoxic compounds, we decided to incorporate π-extended moieties into the N^O$^-$ ligands. Four new Ru(II) complexes (Figure S1), [Ru(bpy)$_2$(dphol)][PF_6] (**1**), [Ru(phen)$_2$(dphol)][PF_6] (**2**), [Ru(bpy)$_2$(hbtz)][PF_6] (**3**), and [Ru(phen)$_2$(hbtz)][PF_6] (**4**) were synthesized and thoroughly characterized. The effect of adding π-extended systems on their cytotoxic properties was investigated in human lung adenocarcinoma (A549) cells, and the mechanism of cytotoxicity was probed using two different biological assays.

EXPERIMENTAL SECTION

General Methods. Standard Schlenk-line techniques under a N_2 atmosphere were used during the preparation of the compounds. Solvents were of reagent grade quality. Ethanol (KOPTEC 200 proof), acetone (EMD Chemicals), dichloromethane (EMD Chemicals), diethyl ether (EMD Chemicals), and glacial acetic acid (EMD Chemicals) were used as received without further purification. $RuCl_3\cdot xH_2O$ (Pressure Chemicals Co.), 2,2′-bipyridine (bpy, Alfa Aesar), 1,10-phenanthroline (phen, Alfa Aesar), 8-hydroxyquinoline (quoH, Acros Organics), 2-(2-hydroxyphenyl)benzothiazole (hbtzH, Sigma-Aldrich), 2,3-diaminophenol (Sigma-Aldrich), 9,10-phenanthrenequinone (Sigma-Aldrich), NH_4PF_6 (Sigma-Aldrich), $NaHCO_3$ (Mallinckrodt), and K_2CO_3 (Spectrum Chemicals) were purchased and used as received. The compounds *cis*-$RuCl_2$(N^N)$_2\cdot 2H_2O$ (N^N = bpy, phen)[28] were prepared following reported procedures.

Instrumentation. The ^{1}H NMR spectra were recorded on an Inova 500 MHz spectrometer. Chemical shifts are reported in δ (ppm) and coupling constants (J) in hertz (Hz). The residual solvent peak was used as an internal reference (δ 7.26 for $CDCl_3$, δ 1.94 for CD_3CN, 2.05 for $(CD_3)_2CO$). Electrospray ionization (ESI) mass spectra were acquired on an Applied Biosystems PE SCIEX QSTAR mass spectrometer (MDS Sciex). Elemental analyses were performed by Atlantic Microlab, Inc. (Norcross, GA). Absorption spectra were recorded on a Shimadzu UVPC-3001 spectrophotometer. Electrochemical measurements were performed under a N_2 atmosphere in dry acetonitrile and 0.1 M tetra-*n*-butylammonium hexafluorophosphate ([^{n}Bu$_4$N][PF_6]) as the supporting electrolyte with a HCH Electrochemical Analyzer model CH 1620A using a BAS Pt disk working electrode, Pt wire auxiliary electrode, and Ag/AgCl (3 M $KCl_{(aq)}$) reference electrode at a 100 mV/s scan rate. The concentration of the Ru complexes for the electrochemical experiments was ∼1 mM. Ferrocene was used as an internal standard and exhibited an $E_{1/2}$ = 0.44 V vs Ag/AgCl for the Fc^+/Fc couple under the same experimental conditions. The $E_{1/2}$ values of the Ru complexes were referenced vs NHE using the following expression: $E_{1/2}$ vs NHE = [($E_{1/2}$ vs Ag/AgCl of Ru complex) + (0.64−0.44)] V, where 0.64 V = $E_{1/2}$ [Fc^+/Fc] vs NHE and 0.44 V = $E_{1/2}$ [Fc^+/Fc] vs Ag/AgCl.

Synthetic Details. *Dibenzo[a,c]phenazin-10-ol (dpholH).* A mixture of 2,3-diaminophenol (210 mg, 1.69 mmol) and 9,10-phenanthrenequinone (336 mg, 1.61 mmol) in 20 mL of ethanol/acetic acid (1:1) was heated to reflux for 2 h. A yellow precipitate was collected by filtration, dissolved in hot dichloromethane (100 mL), and filtered through a short plug of SiO_2. A yellow band was eluted with dichloromethane, and the combined fractions were reduced to ca. 25 mL. After the yellow solution was kept in an ice bath for 30 min, a light yellow precipitate was collected and washed with cold dichloromethane. Yield: 208 mg (44%). ^{1}H NMR (500 MHz, $CDCl_3$): δ 9.39 (dd, 1H, ^3J = 8.0, ^4J = 1.5), 9.29 (dd, 1H, ^3J = 8.0, ^4J = 1.0), 8.57 (m, 2H), 8.15 (s, 1H), 7.87 (dd, 1H, ^3J = 8.5, ^4J = 1.0), 7.84−7.72 (m, 5H), 7.31 (dd, 1H, ^3J = 7.5, ^4J = 1.5). HRMS (ESI+): Calcd for $[C_{20}H_{13}N_2O]^+$ ([M + H]$^+$), 297.1028. Found: 297.1026.

*[Ru(bpy)$_2$(dphol)][PF_6] (**1**).* Samples of *cis*-$RuCl_2$(bpy)$_2\cdot 2H_2O$ (150 mg, 0.29 mmol), dpholH (95 mg, 0.32 mmol), and $NaHCO_3$ (74 mg, 0.88 mmol) were suspended in 70 mL of ethanol and heated to reflux for 8 h. The resulting dark red solution was cooled to room temperature and filtered. A quantity of $NH_4PF_{6(aq)}$ (5 equiv dissolved in 2 mL of water) was added to the filtrate, and a dark red solid precipitated. The solid was dissolved in dichloromethane (50 mL) and washed with water (3 × 30 mL). The organic layer was dried with $MgSO_4$ and reduced to dryness. The residue was dissolved in 10 mL of acetone, and diethyl ether was added slowly until a solid began precipitating. The mixture was stored at 0 °C overnight, during which time a dark red microcrystalline solid formed, which was collected by filtration and washed with diethyl ether (25 mL). Yield: 195 mg (79%). ^{1}H NMR (500 MHz, $(CD_3)_2CO$): δ 9.01 (m, 2H), 8.94 (d, 1H, ^3J = 5.0), 8.86 (d, 1H, ^3J = 8.5), 8.75 (d, 1H, ^3J = 8.5), 8.51 (d, 1H, ^3J = 5.5), 8.47 (d, 1H, ^3J = 8.0), 8.33 (m, 3H), 8.25 (ddd, 1H, ^3J = 8.0, ^3J = 8.0, ^4J = 1.5), 8.16 (d, 1H, ^3J = 8.0), 8.03 (ddd, 1H, ^3J = 8.0, ^3J = 8.0, ^4J = 1.5), 7.87 (ddd, 1H, ^3J = 8.0, ^3J = 8.0, ^4J = 1.5), 7.77 (ddd, 1H, ^3J = 8.5, ^3J = 7.0, ^4J = 1.5), 7.70 (ddd, 1H, ^3J = 8.0, ^3J = 7.0, ^4J = 1.0), 7.66 (m, 2H), 7.61 (ddd, 1H, ^3J = 7.5, ^3J = 5.5, ^4J = 1.5), 7.59 (d, 1H, ^3J = 5.5), 7.41−7.35 (m, 2H), 7.29 (ddd, 1H, ^3J = 7.5, ^3J = 5.5, ^4J = 1.5), 7.24 (dd, 1H, ^3J = 8.0, ^4J = 1.0), 7.18 (ddd, 1H, ^3J = 7.5, ^3J = 5.5, ^4J = 1.5), 7.13 (ddd, 1H, ^3J = 8.5, ^3J = 7.5, ^4J = 1.0), 6.94 (dd, 1H, ^3J = 8.0, ^4J = 1.5). HRMS (ESI+): Calcd for $[C_{40}H_{27}N_6ORu]^+$ ([M−PF_6]$^+$), 709.1290. Found: 709.1287. Anal. Calcd for $C_{40}H_{27}N_6OF_6PRu\cdot 1.05(CH_3)_2CO$: C, 56.66; H, 3.67; N, 9.19. Found: C, 56.84; H, 3.82; N, 9.36.

*[Ru(phen)$_2$(dphol)][PF_6] (**2**).* This compound was prepared in a fashion similar to that described for **1** with *cis*-$RuCl_2$(phen)$_2\cdot 2H_2O$ (151 mg, 0.27 mmol), dpholH (87 mg, 0.19 mmol), and $NaHCO_3$ (69 mg, 0.82 mmol) in ethanol (70 mL). A dark red microcrystalline solid was obtained. Yield: 185 mg (77%). ^{1}H NMR (500 MHz, $(CD_3)_2CO$): δ 9.18 (dd, 1H, ^3J = 5.5, ^4J = 1.0), 9.05 (dd, 1H, ^3J = 8.0, ^4J = 1.0), 8.75 (m, 2H), 8.70 (dd, 1H, ^3J = 8.0, ^4J = 1.0), 8.66 (d, 1H, ^3J = 8.0), 8.49 (dd, 1H, ^3J = 8.0, ^4J = 1.0), 8.41 (dd, 1H, ^3J = 5.5, ^4J = 1.0), 8.36 (d, 2H, ^3J = 8.0), 8.28−8.19 (m, 3H), 8.18 (d, 1H, ^3J = 8.0), 8.11 (d, 1H, ^3J = 9.0), 8.01 (dd, 1H, ^3J = 8.0, ^3J = 5.5), 7.88 (dd, 1H, ^3J = 8.0, ^3J = 5.5), 7.75−7.66 (m, 2H), 7.63 (t, 1H, ^3J = 8.0), 7.56 (dd, 1H, ^3J = 5.5, ^4J = 1.0), 7.46 (dd, 1H, ^3J = 8.0, ^3J = 8.0), 7.29−7.22 (m, 2H), 7.21 (ddd, 1H, ^3J = 8.0, ^3J = 7.0, ^4J = 1.0), 6.87 (dd, 1H, ^3J = 8.0, ^4J = 1.0), 6.44 (t, 1H, ^3J = 7.5). HRMS (ESI+): Calcd for

DOI: 10.1021/acs.inorgchem.8b01988
Inorg. Chem. XXXX, XXX, XXX−XXX

$[C_{44}H_{27}N_6ORu]^+$ ($[M-PF_6]^+$), 757.1290. Found: 757.1284. Anal. Calcd for $C_{44}H_{27}N_6OF_6PRu$: C, 58.61; H, 3.02; N, 9.32. Found: C, 58.60; H, 3.06; N, 9.30.

*[Ru(bpy)$_2$(hbtz)][PF$_6$] (**3**).* This compound was prepared in a fashion similar to that described for **1** with *cis*-$RuCl_2(bpy)_2\cdot 2H_2O$ (158 mg, 0.30 mmol), hbtzH (77 mg, 0.34 mmol), and K_2CO_3 (88 mg, 0.64 mmol) in ethanol/water 1:1 (30 mL) as solvent. A dark red microcrystalline solid was obtained. Yield: 175 mg (73%). ^{1}H NMR (500 MHz, CD_3CN): δ 8.94 (d, 1H, ^3J = 5.5), 8.61 (d, 1H, ^3J = 5.5), 8.43 (d, 1H, ^3J = 8.0), 8.40 (d, 1H, ^3J = 8.0), 8.34 (m, 2H), 8.06 (d, 1H, ^3J = 5.5), 8.01−7.94 (m, 2H), 7.85 (ddd, 1H, ^3J = 8.0, ^3J = 7.5, ^4J = 1.5), 7.82 (d, 1H, ^3J = 8.0), 7.76 (ddd, 1H, ^3J = 8.0, ^3J = 7.5, ^4J = 1.5), 7.57 (dd, 1H, ^3J = 8.0, ^4J = 1.5), 7.47 (ddd, 1H, ^3J = 7.5, ^3J = 5.5, ^4J = 1.5), 7.40 (d, 1H, ^3J = 5.5), 7.34 (ddd, 1H, ^3J = 7.5, ^3J = 5.5, ^4J = 1.5), 7.20−7.11 (m, 3H), 7.02 (ddd, 1H, ^3J = 8.5, ^3J = 7.0, ^4J = 1.5), 6.90 (ddd, 1H, ^3J = 8.5, ^3J = 7.0, ^4J = 1.5), 6.45 (ddd, 1H, ^3J = 8.5, ^3J = 7.0, ^4J = 1.5), 6.40 (d, 1H, ^3J = 8.5), 6.37 (dd, 1H, ^3J = 8.5, ^4J = 1.0). HRMS (ESI+): Calcd for $[C_{33}H_{24}N_5OSRu]^+$ ($[M-PF_6]^+$), 640.0748. Found: 640.0752. Anal. Calcd for $C_{33}H_{24}N_5OF_6PSRu\cdot 0.95(CH_3)_2CO$: C, 51.27; H, 3.56; N, 8.34. Found: C, 51.36; H, 3.55; N, 8.42.

*[Ru(phen)$_2$(hbtz)][PF$_6$] (**4**).* This compound was prepared in a fashion similar to that described for **1** using *cis*-$RuCl_2(phen)_2\cdot 2H_2O$ (177 mg, 0.31 mmol), hbtzH (81 mg, 0.36 mmol), and K_2CO_3 (86 mg, 0.62 mmol) in ethanol/water 1:1 (30 mL). A dark red-green microcrystalline solid was obtained. Yield: 156 mg (60%). ^{1}H NMR (500 MHz, CD_3CN): δ 9.27 (dd, 1H, ^3J = 5.0, ^4J = 1.0), 9.03 (dd, 1H, ^3J = 5.0, ^4J = 1.0), 8.56 (m, 2H), 8.32 (dd, 1H, ^3J = 8.0, ^4J = 1.0), 8.25−8.18 (m, 3H), 8.15 (d, 1H, ^3J = 9.0), 8.11 (d, 1H, ^3J = 9.0), 8.06 (d, 1H, ^3J = 8.5), 7.88 (dd, 1H, ^3J = 8.5, ^3J = 5.0), 7.78−7.73 (m, 2H), 7.62 (dd, 1H, ^3J = 8.0, ^4J = 1.5), 7.46 (dd, 1H, ^3J = 5.5, ^3J = 1.5), 7.34−7.28 (m, 2H), 7.08 (ddd, 1H, ^3J = 8.0, ^3J = 7.0, ^4J = 1.0), 7.00 (ddd, 1H, ^3J = 8.5, ^3J = 7.0, ^4J = 1.5), 6.72 (ddd, 1H, ^3J = 8.5, ^3J = 7.5, ^4J = 1.5), 6.50−6.42 (m, 2H), 6.28 (dd, 1H, ^3J = 8.5, ^4J = 1.0). HRMS (ESI+): Calcd for $[C_{37}H_{24}N_5OSRu]^+$ ($[M-PF_6]^+$), 688.0745. Found: 688.0714. Calcd for $C_{37}H_{24}N_5OF_6PSRu\cdot(CH_3)_2CO$: C, 53.30; H, 3.44; N, 7.97. Found: C, 53.51; H, 3.58; N, 7.89.

*[Ru(bpy)$_2$(quo)][PF$_6$] (**5**).* This compound was prepared in a fashion similar to that described for **1** with *cis*-$RuCl_2(bpy)_2\cdot 2H_2O$ (121 mg, 0.23 mmol), quoH (41 mg, 0.28 mmol), and K_2CO_3 (65 mg, 0.47 mmol) in ethanol/water (1:1, 30 mL). A dark green-red microcrystalline solid was collected by filtration and was washed with diethyl ether (25 mL). Yield: 138 mg (85%). ^{1}H NMR (500 MHz, $(CD_3)_2CO$): δ 8.89 (d, 1H, ^3J = 5.5), 8.74−8.65 (m, 4H), 8.17 (d, 1H, ^3J = 6.0), 8.13−8.04 (m, 4H), 8.00 (m, 2H), 7.89 (d, 1H, ^3J = 5.0), 7.65 (ddd, 1H, ^3J = 7.5, ^3J = 6.0, ^4J = 1.5), 7.55 (dd, 1H, ^3J = 5.0, ^4J = 1.0), 7.46 (m, 1H), 7.40 (m, 2H), 7.32 (t, 1H, ^3J = 8.0), 7.20 (dd, 1H, ^3J = 8.5, ^3J = 5.0), 6.87 (dd, 1H, ^3J = 8.0, ^4J = 1.0), 6.79 (dd, 1H, ^3J = 8.0, ^4J = 1.0). HRMS (ESI+): Calcd for $[C_{29}H_{22}N_5ORu]^+$ ($[M-PF_6]^+$), 558.0868. Found: 558.0866. Calcd for $C_{29}H_{22}N_5OF_6PRu\cdot 0.5(CH_3CH_2)_2O$: C, 50.34; H, 3.68; N, 9.47. Found: C, 50.29; H, 3.79; N, 9.23.

X-ray Crystallography. Single crystals of compounds **1**, **3**, and **4** were obtained by slow diffusion of diethyl ether into acetone solutions of the compounds at room temperature. X-ray data were collected at 110 K on a Bruker APEX II CCD X-ray diffractometer equipped with a graphite monochromated Mo Kα radiation source (λ = 0.71073 Å). The data sets were integrated with the Bruker SAINT software package.[29] The absorption correction (SADABS)[30] was based on fitting a function to the empirical transmission surface as sampled by multiple equivalent measurements. Solution and refinement of the crystal structures were carried out using the SHELX[31] (2013) suite of programs and the graphical interface *ShelXle*[32] was used during the refinement. The structures were solved by the Patterson method; all non-hydrogen atoms were refined with anisotropic displacement parameters using a full-matrix least-squares technique on F^2. Hydrogen atoms were fixed to parent atoms and refined using the riding model.[33,34] PLATON/SQUEEZE was employed in the case of **4** after attempts to model a disordered diethyl ether solvent molecule failed. The solvent molecules in the unit cell (one solvent molecule per asymmetric unit, Z = 4) were determined to occupy 642.9 Å^3. The number of electron counts in voids per unit cell was 159, which is close to that expected for four diethyl ether molecules (168 electrons).

Cell Culture Experiments. The human lung adenocarcinoma A549 cell line, derived from type II pneumocytes (CCL 185), was obtained from American Type Culture Collection (Manassas, VA). Cells were cultured in DMEM/F-12 medium (Dulbecco's Modified Eagle Medium: Nutrient Mixture F-12) with 10% FBS. Cell cultures were incubated in a humidified atmosphere containing 5% CO_2 at 37 °C and were approximately 80% confluent at the time of analysis.

***In vitro* Cytotoxicity.** A549 cells were plated in a 96 well plate and preincubated in a humidified atmosphere containing 5% CO_2 at 37 °C for 24 h. Solutions of the metal complexes in DMEM/F-12 medium were added at different concentrations (final concentrations of compounds: 0−50 μM range, 0.1% DMSO) and the cells were incubated for another 48 h. Cells were then washed twice with PBS and fixed with methanol for 30 min. After fixation, Janus green B (1 mg/mL, Alfa Aesar) was added to each well and incubated at room temperature for 5 min. Cells were washed again twice with PBS and 100 μL of methanol was added to each well to extract the dye. Janus Green B signal was then measured using a BioTek Synergy 4 plate reader set to an absorbance of 630 nm. Two experiments were conducted on different days with each experiment having 8 replicates per concentration. The absorbance of Janus Green B is directly proportional to the number of living cells.

JC-1 Assay. Live cell imaging studies were performed using a Zeiss 510 META NLO multiphoton system consisting of an Axiovert 200 MOT inverted laser scanning confocal microscope (Carl Zeiss Microimaging, Thornwood, NY). A Zeiss Plan-Neofluar 40×/NA = 1.3 oil immersion objective was used to acquire the images.

Cells were plated in Nunc Lab-Tek II chambered coverglass slides (Thermo Scientific) for 24 h prior to treatment with compounds **1**−**4** and cisplatin for 48 h. Cells were then washed with PBS and labeled with the mitochondrial membrane potential probe, JC-1 (Invitrogen) at a final concentration of 5 μg/mL for 30 min at 37 °C. Excitation of JC-1 was performed using an argon ion laser at 488 nm and emission data were collected using a dichroic 545 nm SP in combination with 2 filters 500−550 BP (green signal) and 565−615 BP (red signal). At least eight areas per well were scanned. Two wells were analyzed per treatment. Two experiments were conducted on different days. Ratio (red signal/green signal) was used as an indicator of cellular mitochondria membrane potential.

Calcein AM Assay. Cells were plated in chambered coverglass slides for 24 h prior to treatment with compound **4** or cisplatin for 48 h. Cells were then washed with PBS and incubated with 1 μg/mL Hoeschst 33258 (Invitrogen) and 10 μM acetoxymethyl ester of the membrane-permeable live-cell labeling dye Calcein (calcein AM, Invitrogen) for 30 min, and with 50 nM Mitotracker Deep Red FM (Invitrogen) for 15 min. Following loading, cells were washed and 1 mM cobalt(II) chloride hexahydrate was added to the cells and images were acquired. To collect Hoechst 33258 (Invitrogen) fluorescence, cells were irradiated with the Chameleon tunable Ti:sapphire laser (Coherent Inc., Santa Clara, CA) at an excitation wavelength of 740 nm (which is roughly equivalent to 370 nm in single photon excitation with a continuous wavelength laser system) and emission was collected at 430−480 nm. Calcein was excited with an argon ion laser at 488 nm and emission was monitored using a band-pass 500−530 filter. Mitotracker Deep Red FM was excited with a He−Ne laser at 633 nm and emission was collected using a BP 650−710 filter. Image acquisition was performed sequentially to reduce the possibility of bleed-through between channels. At least eight areas per well were scanned. Two wells were analyzed per treatment. Two experiments were conducted on different days.

Caspase Glo Assay. Cells were cultured for 24 h prior to addition of compound **4** or cisplatin for 48 h. Cells were then washed twice with PBS and 100 μL of the Caspase-Glo 3/7 reagent solution (Promega) was added to each well. Cells were then scanned every 10 min for 30 min and luminescence readings were recorded with

DOI: 10.1021/acs.inorgchem.8b01988
Inorg. Chem. XXXX, XXX, XXX−XXX

BioTek Synergy 4 plate reader. Four wells per concentration were recorded.

RESULTS AND DISCUSSION

Synthesis and Characterization. The precursors for the syntheses of **1**−**5**, namely *cis*-$RuCl_2(N^\wedge N)_2$ (N^N = bpy, phen), were prepared by reacting $RuCl_3{,}xH_2O$ with 2 equiv of N^N in refluxing DMF and in the presence of LiCl (Figure S1).[28] The crude products $[Ru(N^\wedge N)_2(N^\wedge O^-)][PF_6]$ were obtained by reacting *cis*-$RuCl_2(N^\wedge N)_2$ with 1.1 equiv of N^OH (dpholH, hbtzH, and quoH) in refluxing ethanol (or aqueous ethanol) and in the presence of a base ($NaHCO_3$ or K_2CO_3) to deprotonate the phenol moiety of N^OH, followed by precipitation with NH_4PF_6(aq). The five complexes were obtained as dark red microcrystalline solids after recrystallization from acetone/diethyl ether. Although hbtzH is commercially available, surprisingly, there is only one previous report of a Ru(II) complex of the ligand that is similar to **3** but there were no synthetic details or further characterization provided.[35] Due to the C_1 symmetry of **1**−**5**, there are no magnetically equivalent protons in their ^{1}H NMR spectra (Figures S2 and S3); the integration of the signals matches the expected number of protons for each complex (**1**, 27H; **2**, 27H; **3**, 24H; **4**, 24H; **5**, 22H). The identity and purity of the compounds were confirmed by elemental analyses and ESI-MS, where a single peak corresponding to the $[M-PF_6]^+$ cations was observed for all of the complexes (**1**, m/z = 709.1287; **2**, m/z = 757.1284; **3**, m/z = 640.0752; **4**, m/z = 688.0714; **5**, m/z = 558.0866).

X-ray Structures of Compounds 1, 3, and 4. Single crystals of **1**, **3**, and **4** were obtained by slow diffusion of diethyl ether into acetone solutions of the compounds at room temperature. Their X-ray structures are shown in Figures 1 and 2 and the crystallographic data are compiled in Tables S1−S4. Compounds **1** and **3** crystallize in the triclinic space group $P\bar{1}$, whereas **4** crystallizes in the monoclinic space group $P2/n$. There is an interstitial acetone molecule in the asymmetric unit of **1** and **3**. A similar structure of **3** was previously reported in the literature which crystallizes in monoclinic $P2_1/n$ space group with interstitial acetonitrile molecule in the asymmetric unit.[35]

The coordination sphere of the metal center in the structures of the three ruthenium molecules consists of five N atoms and one O atom in a distorted octahedral environment. The Ru−O bond distances are ∼2.060 Å in the three compounds and are similar to the one reported for $[Ru(bpy)_2(quo)][PF_6]$ (**5**; 2.063(6) Å).[36] Their Ru−N bond distances to bpy and phen fall in the 2.019−2.079 Å range and are also in agreement with the respective distances in $[Ru(bpy)_2(quo)][PF_6]$ and Ru(II) polypyridyl compounds in a $[RuN_6]$ coordination environment. In contrast, the Ru−N bond distances to dphol in **1** (Ru−N1, 2.151(3) Å) and to hbtz in **3** (Ru−N5, 2.110(2) Å) and **4** (Ru−N5, 2.110(3) Å) are longer. The elongation of these Ru−N bonds is likely to be caused by steric repulsions between the bulky phenanthrene moiety of dphol and adjacent bpy ligand in the case of **1**, and between the benzothiazolyl moiety of hbtz and adjacent bpy and phen ligands in the case of **3** and **4**, respectively. The dphol ligand in **1** is twisted as depicted in Figure 1, displaying dihedral angles of −30.7(5)° for Ru1−N1−C19−C18 and −19.3(6)° for N1−C19−C18−C17. The hbtz ligands in **3** and **4** are twisted around the C−C bond that connects the phenoxido and benzothiazolyl moieties, exhibiting dihedral angles of 8.5(3)° (N5−C27−C26−C21) and −16.3(5)° (N5−C31−C30−C25), respectively.

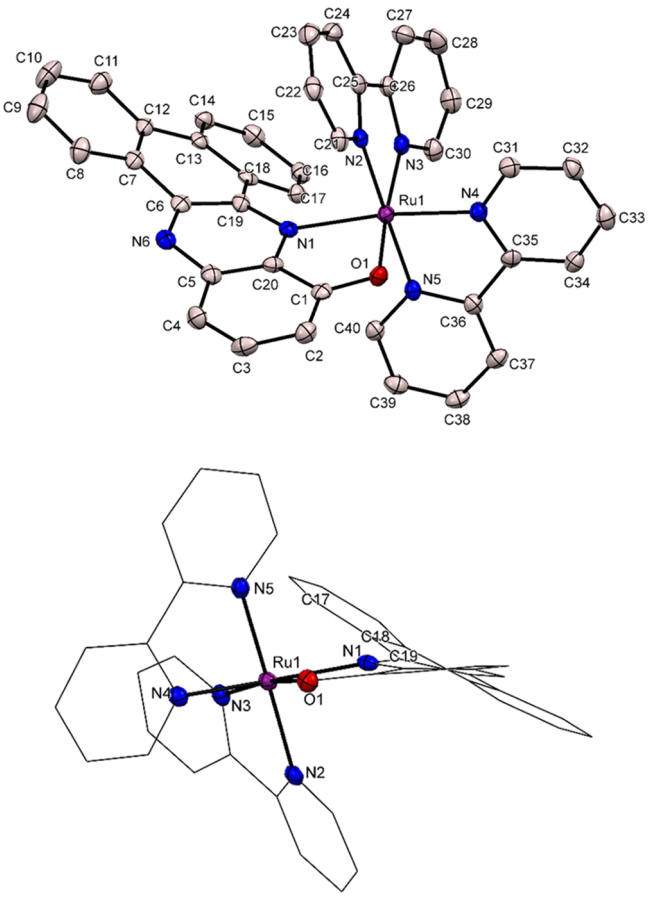

Figure 1. (Top) Thermal ellipsoid plots at the 50% probability level of the X-ray structure of $[Ru(bpy)_2(dphol)][PF_6]$ (**1**). The $[PF_6]^-$ anion and H atoms were omitted for the sake of clarity. (Bottom) Distortion of the dphol ligand in compound **1**.

Electrochemical Properties. The redox properties of complexes **1**−**5** were studied by cyclic voltammetry in acetonitrile. The half-wave potential values ($E_{1/2}$) vs Ag/AgCl were obtained from the cyclic voltammograms of **1**−**5** (Figures S4−S5). The $E_{1/2}$ values were referenced vs NHE for the discussion of the results (NHE = normal hydrogen electrode) as described in the Experimental Section; the values are presented in Table 1. The redox events observed in the cyclic voltammograms of **1**−**5** are quasi-reversible ($i_{pa}/i_{pc} \approx 1$), except for the metal-based oxidation processes for **1** and **2** which are irreversible.

The $Ru^{3+/2+}$ redox couples of **1**−**5** ($E_{1/2}$ $[Ru^{3+/2+}]$ = 0.86−0.74 V range) occur at less positive potentials with respect to $[Ru(bpy)_3]^{2+}$ ($E_{1/2}$ $[Ru]^{3+/2+}$ = 1.54 V[37]). The anionic character and π-donating ability of the O atom donor of the N^O$^-$ ligands destabilize the Ru(dπ) "t_{2g}-type" orbitals (Figure S6) and facilitates metal oxidation. This destabilization effect was verified by DFT calculations reported for the known compound **5**,[38] where the HOMO has contributions from both the Ru(dπ) and O(pπ) orbitals and the HOMO−1 and HOMO−2 are mainly metal-based.

The redox events observed for **5** are in agreement with previous reports of related compounds.[38−40] The metal-based redox couple at $E_{1/2}$ = 0.76 V corresponds to the $Ru^{3+/2+}$ oxidation couple, whereas those at $E_{1/2}$ = −1.28 and −1.53 V

DOI: 10.1021/acs.inorgchem.8b01988
Inorg. Chem. XXXX, XXX, XXX−XXX

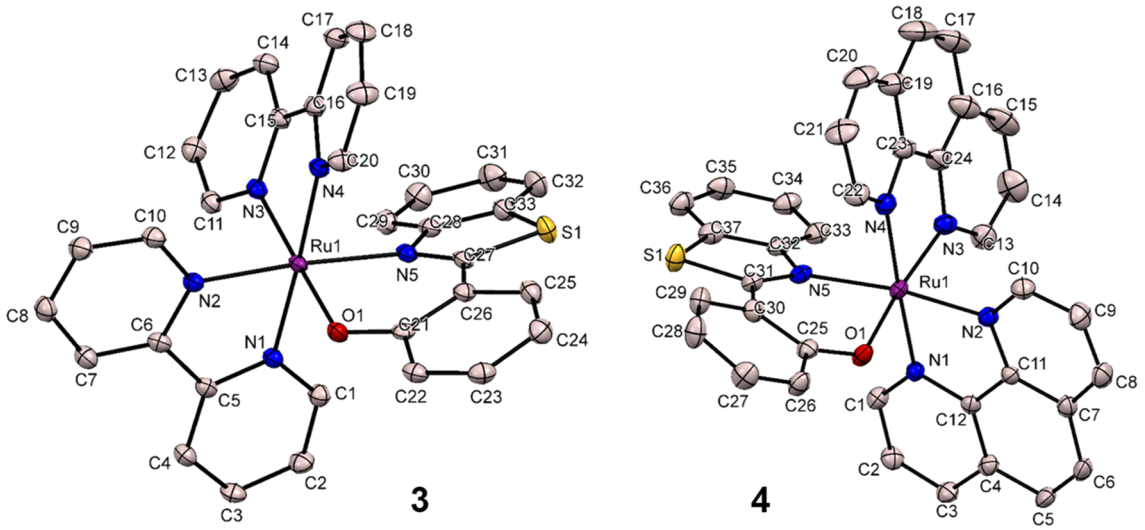

Figure 2. Thermal ellipsoid plots at the 50% probability level of the X-ray structures of $[Ru(bpy)_2(hbtz)][PF_6]$ (**3**) and $[Ru(phen)_2(hbtz)][PF_6]$ (**4**). The $[PF_6]^-$ anion and H atoms were omitted for the sake of clarity.

Table 1. Half Wave Redox Potentials ($E_{1/2}$) of 1−5 Recorded in Acetonitrile

	$E_{1/2}$ (V) vs NHE ($\Delta E = E_{pa} - E_{pc}$ in mV)			
compound	$E_{1/2}$ $[M^{(n+1)+/n+}]^a$	$E_{1/2,red1}$	$E_{1/2,red2}$	$E_{1/2,red3}$
$[Ru(bpy)_2(dphol)][PF_6]$ (1)	0.86[b]	−0.94 (66)	−1.35 (66)	−1.61 (88)
$[Ru(phen)_2(dphol)][PF_6]$ (2)	0.85[b]	−0.93 (64)	−1.36 (85)	−1.59 (80)
$[Ru(bpy)_2(hbtz)][PF_6]$ (3)	0.74 (80)	−1.25 (60)	−1.52 (78)	
$[Ru(phen)_2(hbtz)][PF_6]$ (4)	0.74 (90)	−1.26 (65)	−1.54 (86)	
$[Ru(bpy)_2(quo)][PF6]$ (5)	0.76 (95)	−1.28 (68)	−1.53 (94)	

[a] $Ru^{3+/2+}$ couple for **1**−**5**. [b] Irreversible; the anodic peak potential ($E_{p,a}$) is reported.

correspond to consecutive 1e$^-$ reductions of the bpy ligands. Reduction of quo is not observed in the 1.8 to −1.8 V range of potentials. The $Ru^{3+/2+}$ redox events for **1** and **2** are irreversible and are shifted anodically by ∼100 mV with respect to **5** (Figure S4); i.e., compounds **1** and **2** are more difficult to oxidize than **5**.

The first reduction waves of **1** and **2** ($E_{1/2,red1} \sim -0.94$ V) occur at less negative potentials than that of **5** ($E_{1/2,red1} = -1.28$ V, bpy-based reduction) and are assigned as a reduction of the dphol ligand: dphol + e$^-$ → dphol$^-$. The dphol ligand is easier to reduce than bpy (or quo) due to its more delocalized π-system and it is likely that the electron is delocalized in the phenanthrene moiety. The other two ligand-based reduction waves at ∼ −1.35 and ∼ −1.60 V are assigned as consecutive 1e$^-$ reductions of bpy in the case of **1**, and phen in the case of **2**.

Compounds **3** and **4** display metal-based and ligand-based redox processes at $E_{1/2}$ values very similar to those of **5** (Figure S5). Therefore, it can be concluded that the $E_{1/2}$ $[Ru^{3+/2+}]$ couples of **3** and **4** occur at $E_{1/2} = 0.74$ V and that the ligand-based redox events at $E_{1/2}$ − 1.25 and −1.52 V for **3**, and $E_{1/2}$ − 1.26 and −1.54 V for **4** correspond to consecutive 1e$^-$ reductions of bpy and phen ligands, respectively. The reduction of the hbtz ligand is likely to occur at more negative potentials and is not observed in the potential window of the cyclic voltammogram experiments.

Electronic Properties. The absorption maxima (λ_{abs}) and molar extinction coefficients (ε) for **1**−**5** in acetonitrile are listed in Table 2, and their electronic absorption spectra in acetonitrile are shown in Figures S7−S9. The Ru compounds

Table 2. Electronic Absorption Data for 1−5 Recorded in Acetonitrile

compound	λ_{max}, nm ($\varepsilon \times 10^4$ M^{-1} cm^{-1})
$[Ru(bpy)_2(dphol)][PF_6]$ (1)	710 (0.14), 500 (0.83), 363 (1.92), 292 (4.67), 246 (5.65)
$[Ru(phen)_2(dphol)][PF_6]$ (2)	710 (0.23), 525[a] (1.10), 485 (1.26), 380 (1.80), 355 (2.07), 263 (9.30), 226 (8.26)
$[Ru(bpy)_2(hbtz)][PF_6]$ (3)	652 (0.16), 496 (0.81), 351 (1.35), 292 (4.29)
$[Ru(phen)_2(hbtz)][PF_6]$ (4)	650 (0.20), 480 (1.28), 351 (1.00), 267 (7.14), 225 (7.53)
$[Ru(bpy)_2(quo)][PF6]$ (5)	506 (0.89), 460 (0.65), 394 (0.74) 368 (0.80), 295 (3.47), 252 (3.52)

[a] Shoulder.

with phen as an ancillary ligand (**2** and **4**) exhibit slightly higher molar absorptivity coefficients in the visible region than those with bpy ligands (**1**, **3**, and **5**). The absorption maxima at ∼500 nm for **1**, **3**, and **5** are assigned as singlet metal-to-ligand charge transfer (^{1}MLCT) transitions [Ru(dπ) → bpy(π^*)]. Similarly, broad ^{1}MLCT bands centered in the 480−500 nm interval are observed for **2** and **4**, which arise from Ru(dπ) → phen(π^*) transitions. Such ^{1}MLCT bands for **1**−**5** are red-shifted with respect to the prototype Ru(II) complex $[Ru(bpy)_3]^{2+}$ (^{1}MLCT at 450 nm[37]) due to the destabilization of the Ru-HOMOs (occupied t_{2g}-type orbitals), which in turn decreases the HOMO−LUMO gap and the energy of the MLCT transition, as illustrated in Figure S6. Compounds **1** and **2** exhibit additional absorption features in the 650−800 nm region that are assigned as [Ru(dπ) → dphol(π^*)] ^{1}MLCT transitions. These low energy transitions are in

DOI: 10.1021/acs.inorgchem.8b01988
Inorg. Chem. XXXX, XXX, XXX−XXX

agreement with the less negative reduction potential of coordinated dphol with respect to quo or hbtz, indicating that the π^* MOs of dphol are lower in energy.

The transitions in the 300−400 nm range arise from $^1\pi\pi^*$ ligand-centered (LC) transitions of the N^O$^-$ ligands because the free ligands dpholH (374 and 393 nm), hbtzH (332 nm), and quoH (312 nm) display absorption maxima in this region (Figure S9). The maxima at higher energies (λ < 300 nm) correspond to overlapping L(π) → L(π^*) and bpy(π) → bpy(π^*) LC transitions in the case of **1** (L = dphol), **3** (L = hbtz), and **5** (L = quo), and overlapping L(π) → L(π^*) and phen(π) → phen(π^*) LC transitions for **2** (L = dphol) and **4** (L = hbtz).

Cytotoxic Properties. Compounds **1**−**5** exhibit IC_{50} values in the low micromolar range (Table 3). Cisplatin was used as a positive control (IC_{50} = 6.2 μM). Compound **1** exhibits activity comparable to that of cisplatin, whereas compounds **2**−**4** are more active than the platinum drug. Compound **4** is the most cytotoxic of the Ru series (IC_{50} = 0.8 μM) and is 8-fold more cytotoxic than cisplatin. In sharp contrast, compound **5** is not active in the range of concentrations that were tested (0−50 μM). It is likely that the higher cytotoxicities of **1**−**4** with respect to **5** is due to increased lipophilicities because they feature extended aromatic systems on the ligands dphol (**1** and **2**) and hbtz (**3** and **4**), in support of our initial hypothesis. The higher lipophilicity of dphol and hbtz with respect to quo may increase the cellular uptake of **1**−**4**, as also shown in the work of Meggers[9] and in several studies on the anticancer properties of other Ru[23,4,24−26] complexes.

Table 3. Cytotoxicity Data for Complexes 1−5 against A549 Cells (Using Janus Green B Assay)[a]

compound	IC_{50}, μM (95% CI[b])
$[Ru(bpy)_2(dphol)][PF_6]$ (1)	6.6 (3.2 to 13.9)
$[Ru(phen)_2(dphol)][PF_6]$ (2)	1.3 (0.8 to 2.1)
$[Ru(bpy)_2(hbtz)][PF_6]$ (3)	1.1 (0.7 to 1.9)
$[Ru(phen)_2(hbtz)][PF_6]$ (4)	0.8 (0.5 to 1.2)
$[Ru(bpy)_2(quo)][PF_6]$ (5)	>50
cisplatin	6.2 (2.9 to 13.5)

[a]Compounds **1**−**5** were dissolved in DMEM/F-12 medium (with 0.1% DMSO). Incubation time = 48 h. [b]Values in parentheses represent the 95% confidence interval.

Investigation of the Mechanism of Cancer Cell Death. Disruption and permanent dissipation of the inner mitochondrial transmembrane potential ($\Delta\Psi_m$) is an event that is associated with the intrinsic pathway of apoptosis.[41,42] To determine the effect of **1**−**4** on mitochondria, mitochondrial dysfunction was assessed by measuring the changes in $\Delta\Psi_m$ using JC-1 (5′,6,6′-tetrachloro-1,1′,3,3′-tetraethylbenzimidazolyl carbocyanine iodide).[22,43] JC-1 is a lipophilic cationic dye that accumulates in mitochondria due to the negative potential of the inner membrane on these organelles (−120 to −160 mV[41,44]), and its fluorescence wavelength is potential-dependent: regions within the cell with high mitochondrial polarization (high $\Delta\Psi_m$) are indicated by red fluorescence (590 nm) due to the formation of dye aggregates (so-called J-aggregates). In contrast, green fluorescence (527 nm) of dye monomers is observed when the mitochondria are depolarized (low $\Delta\Psi_m$).[41,45] Therefore, mitochondrial depolarization is indicated by a decrease in the red/green emission intensity ratio (R) of JC-1.[45]

A549 cells were incubated with **1**−**4** at different concentrations for 48 h. Following this period of time, the cells were incubated with JC-1, and R values were calculated. The results are shown in Figure 3. In general, an increase of the concentration of the compounds is accompanied by a progressive decrease of R, indicating that **1**−**4** induce mitochondria depolarization in a dose-dependant fashion, a result that signifies cell death occurs via the intrinsic pathway of apoptosis. To compare the changes of R among **1**−**4**, the change of R (ΔR) with respect to a control (no complex added) was calculated at 5 μM concentration of Ru complex ($\Delta R = [(R_{5\ \mu M} - R_{control})/R_{control}] \times 100\%$). The observed trend is as follows: **4** (−97%) > **2** (−66%) ≈ **3** (−63%) > **1** (−23%), where the values in parentheses represent ΔR. Interestingly, ΔR was directly proportional to the cytotoxicity, where the most cytotoxic compound, **4**, decreases R to the greatest extent. Moreover, **4** induces a greater $\Delta\Psi_m$ depolarization as compared to cisplatin (Figure 4), with ΔR = −70% and −15% for **4** and cisplatin at 1.5 μM concentration, respectively.

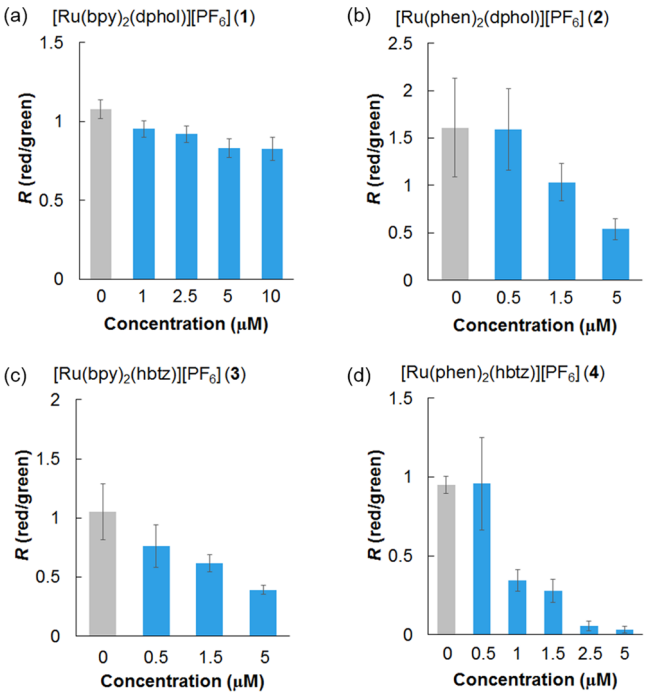

Figure 3. R values from JC-1 assay in A549 cells after 48 h of incubation when exposed to different concentrations of compounds (a) **1**, (b) **2**, (c) **3**, and (d) **4**. The graphs represent means with standard deviation. Control experiments (no metal complex) are depicted in gray.

The typical fibrillar mitochondrial structure in A549 cells is shown in Figure S10, where cells were incubated only with JC-1. Green (Figure S10a) and red (Figure S10b) fluorescence images are shown to highlight the dual emission of JC-1 in mitochondria. Dramatic morphological changes of mitochondria occur when A549 cells are incubated with **4** for 48 h at concentrations as low as **0.5** μM, as shown in Figure 5. Complex **4** induces swelling and fragmentation of mitochondria, producing small and rounded organelles.[41,46] Such morphological changes indicate cell death by the intrinsic

DOI: 10.1021/acs.inorgchem.8b01988
Inorg. Chem. XXXX, XXX, XXX−XXX

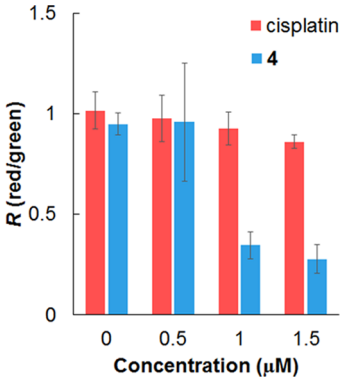

Figure 4. *R* values from JC-1assay in A549 cells after 48 h of incubation when exposed to different concentrations of cisplatin and compound **4**. The graphs represent means with standard deviation.

apoptosis pathway. A progressive decrease of the red fluorescence intensity from J-aggregates can be also seen when the concentration of **4** increases from 0 to 1 μM (Figures 5a–c), indicating loss of $\Delta\Psi_m$ as described previously.

Induction of outer mitochondrial membrane permeabilization (MMP) is a crucial event during cell death via the intrinsic pathway of apoptosis and is often considered as the "point of no return".[41] Such an event is accompanied by a dissipation of $\Delta\Psi_m$ and permeabilization of the inner mitochondrial membrane (IMM). To further support that the intrinsic pathway of apoptosis is triggered by these series of compounds, a biological assay that uses the calcein AM dye was carried out for compound **4**.

In this experiment, A549 cells were loaded with calcein AM and $CoCl_2$. Calcein AM undergoes removal of the ester groups by intracellular esterases to form calcein which gets trapped in cytosolic compartments, including mitochondria.[41] The Co^{II} ions quench the fluorescence of calcein in all subcellular compartments except in mitochondria because the IMM is impermeable to Co^{II} ions and water. When the IMM barriers are functional, a distinct bright green fluorescence signal from calcein identifies mitochondria,[41] as can be observed in Figure 6a. Dim green fluorescence from calcein is observed elsewhere because Co^{II} ions quench calcein fluorescence. The signal from calcein overlays very well with the red fluorescence from Mitotracker, a mitochondria-specific fluorescent dye, thus confirming the localization of calcein in mitochondria (Figures 6a–c). In contrast, incubation of A549 cells with 1 μM **4** for 48 h leads to calcein fluorescence quenching inside mitochondria, and dim green fluorescence is observed throughout the cells (Figure 7). These results indicate long-lasting opening of the mitochondrial permeability transition pore (MPTP) complex, which allows Co^{II} ions to enter the mitochondrial matrix and quench calcein fluorescence, thus supporting the intrinsic pathway of apoptosis as the mechanism of cancer cell death.

Caspases are cysteine proteases that are involved in both the initiation and execution phases of apoptosis and, indeed, the activation of these proteolytic enzymes is often taken as a hallmark of apoptosis.[47,48] In particular, caspase-3/7, known as the executioner caspases, are activated after cytochrome c leaks out of mitochondria when a cell dies via the intrinsic pathway of apoptosis.[41] The effect of a chemotherapy drug on the activity of caspase-3/7 can be examined using the Caspase-Glo assay kit, which includes (i) the caspase-3/7 substrate DEVD-NH-luciferin and (ii) the Luciferase enzyme. Caspase-3/7, which are activated during apoptosis, cleave the amino acid sequence DEVD (Asp-Glu-Val-Asp), releasing 6-aminoluciferin (Figure S11). The latter undergoes oxidative decarboxylation catalyzed by the Luciferase enzyme, producing oxyluciferin in an electronically excited state (oxyluciferin*), which emits light ($h\nu$) when it is deactivated and returns to the ground state (oxyluciferin* → oxyluciferin + $h\nu$). The luminescence intensity is proportional to the amount of caspase-3/7 activity.

A549 cells were treated with compound **4** at three different concentrations (0.75, 1.5, and 2.25 μM) for 48 h, and caspase-3/7 activity was determined after this period of time. Compound **4** induced caspase-3/7 activity in a concentration-dependent fashion as depicted in Figure 8, in which an increase in the oxyluciferin luminescence intensity is observed upon increasing the concentration of **4**, results that confirm that this Ru compound induces cell suicide via the intrinsic pathway. The data in Figure 8 show that a lower concentration of **4** is needed to induce caspase-3/7 activity with respect to cisplatin, in which 2.25 μM **4** reaches activity comparable to that of 6.25 μM cisplatin, indicating higher apoptosis inducing ability of **4**.

CONCLUSIONS

The lack of studies in the literature of cytotoxic properties of Ru(II) polypyridyl complexes in a $[Ru^{II}N_5O]^+$ coordination

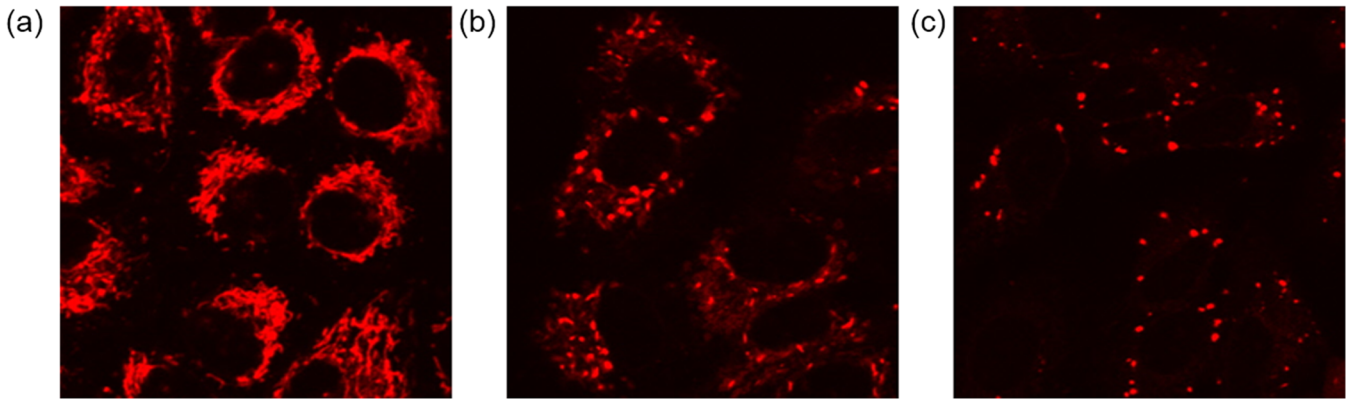

Figure 5. Confocal red fluorescence images of JC-1 in A549 cells incubated with (a) 0, (b) 0.5, and (c) 1 μM of compound **4**. Only red fluorescence images were shown to emphasize the progressive decrease of red fluorescence intensity with concentration. Field of view = 75 × 75 μm. Images were collected after 48 h of incubation with the corresponding concentration of the compound.

DOI: 10.1021/acs.inorgchem.8b01988
Inorg. Chem. XXXX, XXX, XXX–XXX

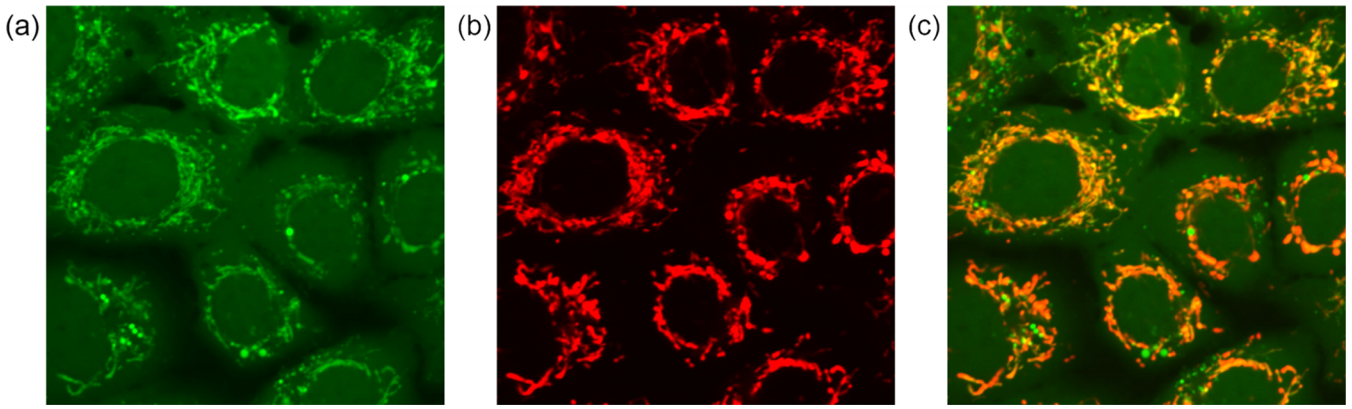

Figure 6. Confocal fluorescence images of A549 cells coincubated with Calcein AM and Mitotracker in the absence of compound **4**. (a) Green fluorescence from Calcein (+$CoCl_2$), (b) red fluorescence from Mitotracker, and (c) overlay of (a, b) images. Field of view = 75 × 75 μm. Images were collected after 48 h of incubation.

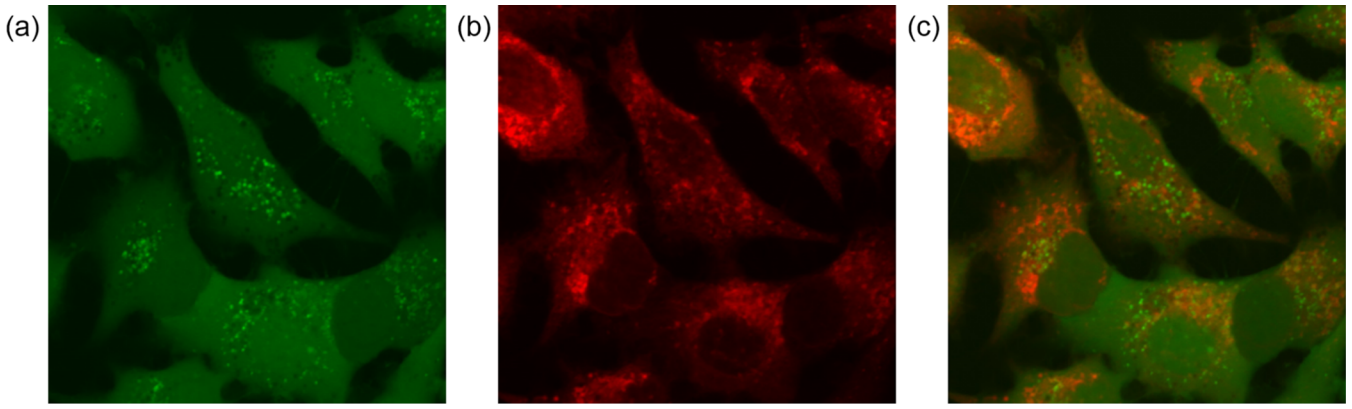

Figure 7. Confocal fluorescence images of A549 cells coincubated with compound **4** (1 μM), Calcein AM, and Mitotracker. (a) Green fluorescence from Calcein AM (+$CoCl_2$), (b) red fluorescence from Mitotracker, and (c) overlay of (a, b) images. Field of view = 75 × 75 μm. Images were collected after 48 h of incubation with the compound.

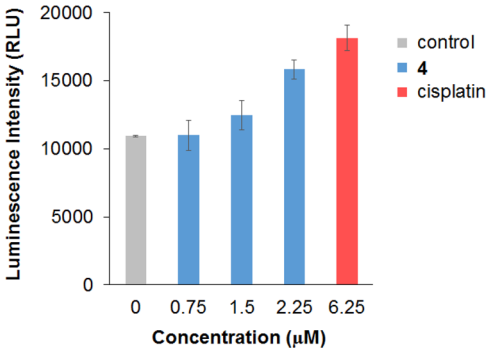

Figure 8. Caspase-3/7 activity measurements when A549 cells are exposed for 48 h to compound **4** or cisplatin. The graphs represent means with standard deviation.

environment prompted us to explore the biological activities of a new series of Ru polypyridyl compounds with the N^O$^-$ bidentate ligands dphol and hbtz. Four new Ru complexes (**1**−**4**) were prepared and characterized by ^{1}H NMR spectroscopy, mass spectrometry, elemental analysis, and X-ray crystallography. The ^{1}MLCT transitions for these complexes are bathochromically shifted with respect to that of $[Ru(bpy)_3]^{2+}$ due to the π-donating ability of the O$^-$-donor of N^O$^-$, which destabilizes the Ru(dπ) HOMOs and decreases the energy of the Ru(dπ) → L(π*) transition. This effect is also reflected in the less positive oxidation potential for this series of compounds with respect to the prototype complex $[Ru(bpy)_3]^{2+}$.

The four compounds are cytotoxic against human lung adenocarcinoma (A549) cells with IC_{50} values in the low micromolar range. Compound **4**, the most active of the series, is ∼8 times more cytotoxic than cisplatin in this cell line. The four Ru complexes induce loss of $\Delta\Psi_m$ in a concentration-dependent fashion, and the cytotoxicity of **1**−**4** is directly proportional to the loss of $\Delta\Psi_m$, indicating that **1**−**4** induce apoptosis via the intrinsic pathway in A549 cells. Moreover, compound **4** promotes the long-lasting opening of the MPTP complex and induces the activity of caspase-3/7, confirming that A549 cells die by the intrinsic pathway of apoptosis when incubated with this type of Ru complex. These results support the hypothesis that increasing the lipophilicity of the N^O$^-$ ligand is a successful strategy for accessing a new family of pro-apoptotic Ru complexes with a $[Ru^{II}N_5O]^+$ coordination environment. This work complements the strategy[23] to increase cellular uptake and anticancer activity. These results are expected to encourage the exploration of the anticancer activities of other octahedral Ru(II) polypyridyl complexes possessing coordination environments different than $[Ru^{II}N_6]^{2+}$.

DOI: 10.1021/acs.inorgchem.8b01988
Inorg. Chem. XXXX, XXX, XXX−XXX

■ ASSOCIATED CONTENT

Supporting Information

The Supporting Information is available free of charge on the ACS Publications website at DOI: 10.1021/acs.inorgchem.8b01988.

Reaction schemes, NMR spectra, crystallographic data and refinement parameters, bond distances and bond angles, cyclic voltammograms, electronic absorption spectra, and confocal fluorescence microscopy images (PDF)

Accession Codes

CCDC 997833−997835 contain the supplementary crystallographic data for this paper. These data can be obtained free of charge via www.ccdc.cam.ac.uk/data_request/cif, by emailing data_request@ccdc.cam.ac.uk, or by contacting The Cambridge Crystallographic Data Centre, 12 Union Road, Cambridge CB2 1EZ, UK; fax: +44 1223 336033.

■ AUTHOR INFORMATION

Corresponding Author

*E-mail: dunbar@chem.tamu.edu.

ORCID

Sayan Saha: 0000-0002-6724-6430

Notes

The authors declare no competing financial interest.

■ ACKNOWLEDGMENTS

Confocal microscopy studies were performed in the Texas A&M University College of Veterinary Medicine & Biomedical Sciences Image Analysis Laboratory, supported by NIH-NCRR (Grant 1S10RR22532-01). K.R.D. thanks the National Science Foundation (Grant CHE-12465067) for support of this work.

■ REFERENCES

(1) Kelland, L. The resurgence of platinum-based cancer chemotherapy. *Nat. Rev. Cancer* **2007**, *7* (8), 573−584.

(2) Wheate, N. J.; Walker, S.; Craig, G. E.; Oun, R. The status of platinum anticancer drugs in the clinic and in clinical trials. *Dalton Trans.* **2010**, *39* (35), 8113−8127.

(3) Groessl, M.; Reisner, E.; Hartinger, C. G.; Eichinger, R.; Semenova, O.; Timerbaev, A. R.; Jakupec, M. A.; Arion, V. B.; Keppler, B. K. Structure−Activity Relationships for NAMI-A-type Complexes (HL)[trans-$RuCl_4L$(S-dmso)ruthenate(III)] (L = Imidazole, Indazole, 1,2,4-Triazole, 4-Amino-1,2,4-triazole, and 1-Methyl-1,2,4-triazole): Aquation, Redox Properties, Protein Binding, and Antiproliferative Activity. *J. Med. Chem.* **2007**, *50* (9), 2185−2193.

(4) Trondl, R.; Heffeter, P.; Kowol, C. R.; Jakupec, M. A.; Berger, W.; Keppler, B. K. NKP-1339, the first ruthenium-based anticancer drug on the edge to clinical application. *Chem. Sci.* **2014**, *5* (8), 2925−2932.

(5) Leijen, S.; Burgers, S. A.; Baas, P.; Pluim, D.; Tibben, M.; van Werkhoven, E.; Alessio, E.; Sava, G.; Beijnen, J. H.; Schellens, J. H. M. Phase I/II study with ruthenium compound NAMI-A and gemcitabine in patients with non-small cell lung cancer after first line therapy. *Invest. New Drugs* **2015**, *33* (1), 201−214.

(6) Bergamo, A.; Sava, G. Linking the future of anticancer metal-complexes to the therapy of tumour metastases. *Chem. Soc. Rev.* **2015**, *44* (24), 8818−8835.

(7) Gransbury, G. K.; Kappen, P.; Glover, C. J.; Hughes, J. N.; Levina, A.; Lay, P. A.; Musgrave, I. F.; Harris, H. H. Comparison of KP1019 and NAMI-A in tumour-mimetic environments. *Metallomics* **2016**, *8* (8), 762−773.

(8) Bergamo, A.; Pelillo, C.; Chambery, A.; Sava, G. Influence of components of tumour microenvironment on the response of HCT-116 colorectal cancer to the ruthenium-based drug NAMI-A. *J. Inorg. Biochem.* **2017**, *168*, 90−97.

(9) Havrylyuk, D.; Heidary, D. K.; Nease, L.; Parkin, S.; Glazer, E. C. Photochemical Properties and Structure−Activity Relationships of RuII Complexes with Pyridylbenzazole Ligands as Promising Anticancer Agents. *Eur. J. Inorg. Chem.* **2017**, *2017* (12), 1687−1694.

(10) Lenis-Rojas, O. A.; Roma-Rodrigues, C.; Fernandes, A. R.; Marques, F.; Pérez-Fernández, D.; Guerra-Varela, J.; Sánchez, L.; Vázquez-García, D.; López-Torres, M.; Fernández, A.; Fernández, J. J. Dinuclear $Ru^{II}(bipy)_2$ Derivatives: Structural, Biological, and in Vivo Zebrafish Toxicity Evaluation. *Inorg. Chem.* **2017**, *56* (12), 7127−7144.

(11) Schatzschneider, U.; Niyhesel, J.; Ott, I.; Gust, R.; Alborzinia, H.; Wölfl, S. Cellular Uptake, Cytotoxicity, and Metabolic Profiling of Human Cancer Cells Treated with Ruthenium(II) Polypyridyl Complexes $[Ru(bpy)_2(N\text{-}N)]Cl_2$ with N-N = bpy, phen, dpq, dppz, and dppn. *ChemMedChem* **2008**, *3* (7), 1104−1109.

(12) Schäfer, S.; Ott, I.; Gust, R.; Sheldrick, W. S. Influence of the Polypyridyl (pp) Ligand Size on the DNA Binding Properties, Cytotoxicity and Cellular Uptake of Organoruthenium(II) Complexes of the Type $[(\eta^6\text{-}C_6Me_6)Ru(L)(pp)]^{n+}$ [L = Cl, n = 1; L = $(NH_2)_2CS$, n = 2]. *Eur. J. Inorg. Chem.* **2007**, *2007*, 3034−3046.

(13) Tan, C.; Lai, S.; Wu, S.; Hu, S.; Zhou, L.; Chen, Y.; Wang, M.; Zhu, Y.; Lian, W.; Peng, W.; Ji, L.; Xu, A. Nuclear Permeable Ruthenium(II) β-Carboline Complexes Induce Autophagy To Antagonize Mitochondrial-Mediated Apoptosis. *J. Med. Chem.* **2010**, *53* (21), 7613−7624.

(14) Tan, C.; Wu, S.; Lai, S.; Wang, M.; Chen, Y.; Zhou, L.; Zhu, Y.; Lian, W.; Peng, W.; Ji, L.; Xu, A. Synthesis, structures, cellular uptake and apoptosis-inducing properties of highly cytotoxic ruthenium-Norharman complexes. *Dalton Trans.* **2011**, *40* (34), 8611−8621.

(15) Qian, C.; Wang, J.-Q.; Song, C.-L.; Wang, L.-L.; Ji, L.-N.; Chao, H. The induction of mitochondria-mediated apoptosis in cancer cells by ruthenium(ii) asymmetric complexes. *Metallomics* **2013**, *5* (7), 844−854.

(16) Garner, R. N.; Gallucci, J. C.; Dunbar, K. R.; Turro, C. $[Ru(bpy)_{2(}5\text{-cyanouracil})_2]^{2+}$ as a Potential Light-Activated Dual-Action Therapeutic Agent. *Inorg. Chem.* **2011**, *50*, 9213−9215.

(17) Respondek, T.; Garner, R. N.; Herroon, M. K.; Podgorski, I.; Turro, C.; Kodanko, J. J. Light Activation of a Cysteine Protease Inhibitor: Caging of a Peptidomimetic Nitrile with RuII(bpy)2. *J. Am. Chem. Soc.* **2011**, *133*, 17164−17167.

(18) Sears, R. B.; Joyce, L. E.; Ojaimi, M.; Gallucci, J. C.; Thummel, R. P.; Turro, C. Photoinduced ligand exchange and DNA binding of cis-$[Ru(phpy)(phen)(CH_3CN)_2]^+$ with long wavelength visible light. *J. Inorg. Biochem.* **2013**, *121*, 77−87.

(19) Sgambellone, M. A.; David, A.; Garner, R. N.; Dunbar, K. R.; Turro, C. Cellular Toxicity Induced by the Photorelease of a Caged Bioactive Molecule: Design of a Potential Dual-Action Ru(II) Complex. *J. Am. Chem. Soc.* **2013**, *135*, 11274−11282.

(20) Komor, A. C.; Barton, J. K. The path for metal complexes to a DNA target. *Chem. Commun.* **2013**, *49*, 3617−3630.

(21) Gill, M. R.; Thomas, J. A. Ruthenium(II) polypyridyl complexes and DNA-from structural probes to cellular imaging and therapeutics. *Chem. Soc. Rev.* **2012**, *41*, 3179−3192.

(22) Pierroz, V.; Joshi, T.; Leonidova, A.; Mari, C.; Schur, J.; Ott, I.; Spiccia, L.; Ferrari, S.; Gasser, G. Molecular and Cellular Characterization of the Biological Effects of Ruthenium(II) Complexes Incorporating 2-Pyridyl-2-pyrimidine-4-carboxylic Acid. *J. Am. Chem. Soc.* **2012**, *134*, 20376−20387.

(23) Mulcahy, S. P.; Grundler, K.; Frias, C.; Wagner, L.; Prokop, A.; Meggers, E. Discovery of a strongly apoptotic ruthenium complex through combinatorial coordination chemistry. *Dalton Trans.* **2010**, *39*, 8177−8182.

(24) Heidary, D. K.; Howerton, B. S.; Glazer, E. C. Coordination of Hydroxyquinolines to a Ruthenium Bis-dimethyl-phenanthroline Scaffold Radically Improves Potency for Potential as Antineoplastic Agents. *J. Med. Chem.* **2014**, *57* (21), 8936−8946.

DOI: 10.1021/acs.inorgchem.8b01988
Inorg. Chem. XXXX, XXX, XXX−XXX

(25) Yang, L.; Zhang, J.; Wang, C.; Qin, X.; Yu, Q.; Zhou, Y.; Liu, J. Interaction between 8-hydroxyquinoline ruthenium(ii) complexes and basic fibroblast growth factors (bFGF): inhibiting angiogenesis and tumor growth through ERK and AKT signaling pathways. *Metallomics* **2014**, *6* (3), 518−531.
(26) Zhang, Y.; Zhou, Q.; Zheng, Y.; Li, K.; Jiang, G.; Hou, Y.; Zhang, B.; Wang, X. DNA Photocleavage by Non-innocent Ligand-Based Ru(II) Complexes. *Inorg. Chem.* **2016**, *55* (9), 4296−4300.
(27) Zhang, Y.; Zhou, Q.; Tian, N.; Li, C.; Wang, X. Ru(II)-Complex-Based DNA Photocleaver Having Intense Absorption in the Phototherapeutic Window. *Inorg. Chem.* **2017**, *56* (4), 1865−1873.
(28) Sullivan, B. P.; Salmon, D. J.; Meyer, T. Mixed Phosphine 2,2′-Bipyridine Complexes of Ruthenium. *Inorg. Chem.* **1978**, *17*, 3334−3341.
(29) *SMART and SAINT*; Siemens Analytical X-ray Instruments Inc.: Madison, WI, 1996.
(30) Sheldrick, G. M. *SADABS*; University of Gottinggen: Gottingen, Germany, 1996.
(31) Sheldrick, G. A short history of SHELX. *Acta Crystallogr., Sect. A: Found. Crystallogr.* **2008**, *64* (1), 112−122.
(32) Hubschle, C. B.; Sheldrick, G. M.; Dittrich, B. ShelXle: a Qt graphical user interface for SHELXL. *J. Appl. Crystallogr.* **2011**, *44* (6), 1281−1284.
(33) Dolomanov, O. V.; Bourhis, L. J.; Gildea, R. J.; Howard, J. A. K.; Puschmann, H. OLEX2: a complete structure solution, refinement and analysis program. *J. Appl. Crystallogr.* **2009**, *42* (2), 339−341.
(34) Sheldrick, G. Crystal structure refinement with SHELXL. *Acta Crystallogr., Sect. C: Struct. Chem.* **2015**, *71* (1), 3−8.
(35) Keyes, T. E.; Leane, D.; Forster, R. J.; Coates, C. G.; McGarvey, J. J.; Nieuwenhuyzen, M. N.; Figgemeier, E.; Vos, J. G. Redox and Spectroscopic Orbitals in Ru(II) and Os(II) Phenolate Complexes. *Inorg. Chem.* **2002**, *41* (22), 5721−5732.
(36) Brissard, M.; Convert, O.; Gruselle, M.; Guyard-Duhayon, C.; Thouvenot, R. Enantiospecific Synthesis of Δ and Λ $[Ru(bpy)_2ppy]^+$ and $[Ru(bpy)_2quo]^+$ (bpy = 2,2′-Bipyridine, ppy = Phenylpyridine$^-H^+$, quo = 8-Hydroxyquinolate): ^1H and ^{13}C NMR Studies and X-ray Structure Determination of *rac*-$[Ru(bpy)_2quo]PF_6$. *Inorg. Chem.* **2003**, *42*, 1378−1385.
(37) Sun, Y.; Joyce, L. E.; Dickson, N. M.; Turro, C. Efficient DNA photocleavage by $[Ru(bpy)_2(dppn)]^{2+}$ with visible light. *Chem. Commun.* **2010**, *46*, 2426−2428.
(38) Zhao, H. C.; Harney, J. P.; Huang, Y.-T.; Yum, J.-H.; Nazeeruddin, M. K.; Grätzel, M.; Tsai, M.-K.; Rochford, J. Evaluation of a Ruthenium Oxyquinolate Architecture for Dye-Sensitized Solar Cells. *Inorg. Chem.* **2012**, *51*, 1−3.
(39) Bhattacharya, S. 8-quinolinolate Complexes of Ruthenium(II). Synthesis, Characterization and Electron Transfer Properties. *Polyhedron* **1993**, *12* (2), 235−239.
(40) Pramanik, N. C.; Bhattacharya, S. Bis(quinolin-8-olato) Complexes of Ruthenium. Synthesis,Characterization and Cyclic Voltammetric Studies. *J. Chem. Res., Synop.* **1997**, 98−99.
(41) Kroemer, G.; Galluzzi, L.; Brenner, C. Mitochondrial Membrane Permeabilization in Cell Death. *Physiol. Rev.* **2007**, *87*, 99−163.
(42) Boehning, D.; Patterson, R. L.; Sedaghat, L.; Glebova, N. O.; Kurosaki, T.; Snyder, S. H. Cytochrome c binds to inositol (1,4,5) trisphosphate receptors, amplifying calcium-dependent apoptosis. *Nat. Cell Biol.* **2003**, *5* (12), 1051−1061.
(43) Qian, C.; Wang, J.-Q.; Song, C.-L.; Wang, L.-L.; Ji, L.-N.; Chao, H. The induction of mitochondria-mediated apoptosis in cancer cells by ruthenium(II) asymmetric complexes. *Metallomics* **2013**, *5*, 844−854.
(44) Lemasters, J. J.; Ramshesh, V. K. Imaging of mitochondrial polarization and depolarization with cationic fluorophores. *Methods Cell Biol.* **2007**, *80*, 283−295.
(45) Johnson, I.; Spence, M. T. Z. The Molecular Probes Handbook: A Guide to Fluorescent Probes and Labeling Technologies. http://www.lifetechnologies.com/ipac/en/home/references/molecular-probes-the-handbook.html (accessed 17 Jan 2014).
(46) Cao, R.; Jia, J.; Ma, X.; Zhou, M.; Fei, H. Membrane Localized Iridium(III) Complex Induces Endoplasmic Reticulum Stress and Mitochondria-Mediated Apoptosis in Human Cancer Cells. *J. Med. Chem.* **2013**, *56*, 3636−3644.
(47) Li, J.; Yuan, J. Caspases in apoptosis and beyond. *Oncogene* **2008**, *27*, 6194−6206.
(48) Tan, C.; Wu, S.; Lai, S.; Wang, M.; Chen, Y.; Zhou, L.; Zhu, Y.; Lian, W.; Peng, W.; Ji, L.; Xu, A. Synthesis, structures, cellular uptake and apoptosis-inducing properties of highly cytotoxic ruthenium-Norharman complexes. *Dalton Trans.* **2011**, *40*, 8611−8621.

DOI: 10.1021/acs.inorgchem.8b01988
Inorg. Chem. XXXX, XXX, XXX−XXX